

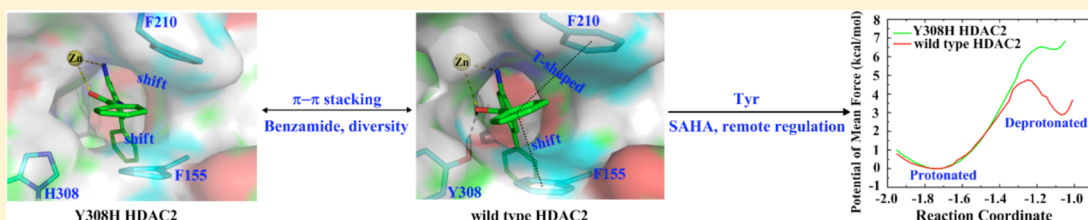
Structure–Function Analysis of the Conserved Tyrosine and Diverse π -Stacking among Class I Histone Deacetylases: A QM (DFT)/MM MD Study

Jingwei Zhou,[†] Hujun Xie,[‡] Zhihong Liu,[†] Hai-Bin Luo,^{*,†} and Ruibo Wu^{*,†}

[†]School of Pharmaceutical Sciences, Sun Yat-sen University, Guangzhou, 510006 Guangdong, P.R. China

[‡]School of Food Science and Biotechnology, Zhejiang Gongshang University, Hangzhou, 310035 Zhejiang, P.R. China

Supporting Information



ABSTRACT: Discovery of the isoform-selective histone deacetylases (HDACs) inhibitors is of great medical importance and still a challenge. The comparison studies on the structure–function relationship of the conserved residues, which are located in the linker binding channel among class I HDACs (including 4 isoforms: HDAC1/2/3/8), have been carried out by using *ab initio* QM/MM MD simulations, a state-of-the-art approach to simulate metallo-enzymes. We found that the conserved tyrosine (Y303/308/286/306 in HDAC1/2/3/8, respectively) could modulate the zinc-inhibitor chelation among all class I HDACs with different regulatory mechanisms. For HDAC1/2/3 selective-inhibitor benzamide, the conserved tyrosine could modulate the coordinative ability of the central atom (Zn^{2+}), while for pan-inhibitor SAHA, the conserved tyrosine could increase the chelating ability of the ligand (SAHA). Moreover, it is first found that the conserved tyrosine is correlated with the intertransformation of π – π stacking styles (parallel shift vs T-shaped) by the aromatic ring in benzamide and the two conserved phenylalanine residues of HDACs. In addition, the catalytic roles of the conserved tyrosine in stabilizing the transition state and intermediate are further revealed. These findings provide useful molecular basis knowledge for further isoform-selective inhibitor design among class I HDACs.

1. INTRODUCTION

Histone deacetylases (HDACs), which are involved in the removal of acetyl groups from acetyl-lysine residues of N-terminal tails of histone and other cellular proteins, have been shown to activate transcription of genes regulating cellular expression, differentiation, and apoptosis.^{1–7} Evidence indicates that dysregulation of HDACs is a common feature associated with cancer and a wide range of other human disorders including inflammation, neurological and cardiovascular diseases, metabolic disorders, even neurodegenerative diseases of aging (such as Amyotrophic lateral sclerosis and Alzheimer’s disease), and psychiatric conditions (such as schizophrenia).^{8–16} Importantly, blocking HDACs with HDAC inhibitors (HDACi) has been shown to be a quite promising strategy for the development of new therapeutics against these diseases.^{17–24} So far, a variety of HDACi, i.e., entinostat (MS-275), valproic acid (VPA), and Mocetinostat (MGCD-0103), have been evaluated in several clinical trials,^{25–29} and the broad-spectrum inhibitors SAHA³⁰ (vorinostat, Merck) and FK-228^{31,32} (romidepsin, Cloucester) have already been approved as anticancer drugs to treat cutaneous T-cell lymphoma (CTCL). However, it is still of great medical

importance and challenge to develop selective HDACi to overcome side effects, which mostly come from the pan-inhibitory effect on HDACs.^{8,11,33–41}

According to phylogenetic sequence and function, all 11 known isoforms of zinc-dependent HDACs in humans have been divided into three classes^{17,42,43} with HDAC1/2/3/8 belonging to class I. For all class I HDACs, as shown in Figure 1, a strong hydrogen bond is formed between the chelator of HDACi and the conserved tyrosine (Y303/308/286/306 in HDAC1/2/3/8, respectively) located at the bottom of the linker binding channel.^{44–48} Mutation of the Y306/Y303 to F306/F303 in HDAC8/1 would bring the decrease of catalytic activity in previous experimental studies.^{47,49} Moreover, experimental studies have shown that mutation of the histidine (converted in class II HDACs) to tyrosine (converted in class I HDACs) would significantly increase enzyme activity as well as its binding to hydroxamate LAQ-824 in HDAC4/7.^{33,50–52} So far, the rate-limiting step of the catalytic deacetylation reaction in HDAC8 has been found in our previously combined

Received: August 22, 2014



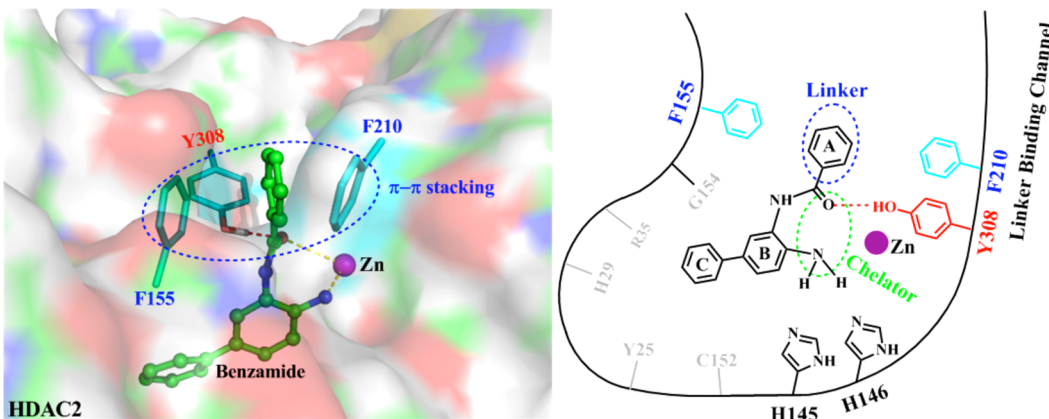


Figure 1. Illustration of the π - π stacking and the conserved tyrosine residue in the linker binding channel for class I HDACs (HDAC1/2/3/8, take HDAC2 for example).

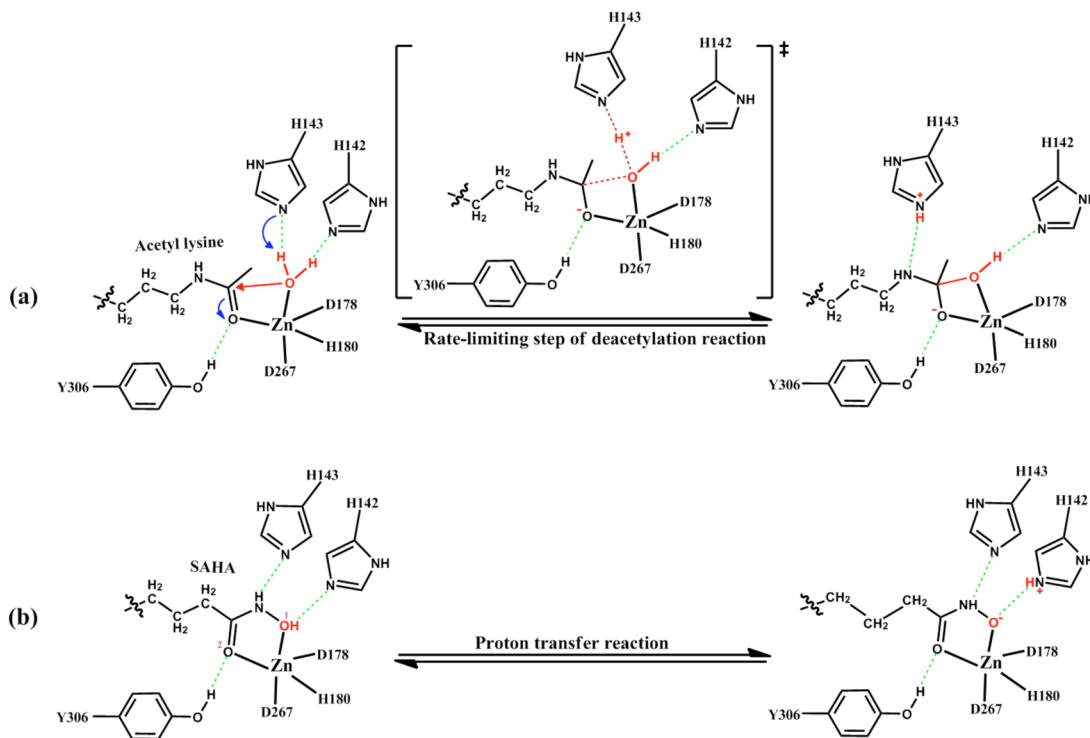


Figure 2. Illustration of the rate-limiting step of the deacetylation reaction for substrate (a) and the possible reversible proton transfer reaction for pan-inhibitor SAHA (b) in HDAC8.

quantum mechanism/molecular mechanism (QM/MM) molecular dynamics (MD) simulations,⁵³ as shown in Figure 2(a). Nevertheless, the exact catalytic role of this tyrosine is still unknown. Meanwhile, compared to the pK_a value of aliphatic hydroxamic acids in free state which is 9.4, the computational study of the zinc complexation of hydroxamic acids in TACE suggests that their acidity increases by ~ 3.3 pK_a units upon binding to the zinc ion, and thus it was suggested that maybe the hydroxamic acids ought to be deprotonated (negative charged) by H142 upon binding to the zinc ion,^{33,54} leading to stronger zinc-SAHA chelating ability. However, our recent QM/MM MD simulations suggested that SAHA prefers to be protonated (neutral charged) due to the proton transfer reaction of SAHA in HDAC8 being unfavorable with the endothermicity of 3.8 kcal/mol.⁵⁵ Therefore, it is essential to further elucidate the catalytic role of the conserved tyrosine

both in the deacetylation reaction of the substrate and the proton transfer reaction of SAHA among class I HDACs.

As shown in Figure 1, the two conserved phenylalanines (F150/205 in HDAC1, F155/210 in HDAC2, F133/188 in HDAC3, and F152/208 in HDAC8), located at the entrance of the linker binding channel, serve as an important water gating factor to affect the hydrophobicity of the active pocket through π -stacking with the linker of HDACi. In contrast, the π - π stacking conformation of the two conserved phenylalanines is destroyed and the conserved tyrosine is replaced by a histidine in class II HDACs, leading to a decrease of the zinc coordinative ability as observed in crystal structures,^{50,52} which has also been proven in our previous QM/MM MD simulations.⁵⁵ Meanwhile, many other significant efforts involving the linker binding channel had been reported.^{33,49–52,54,56,57} Nevertheless, it is lack of the structure–

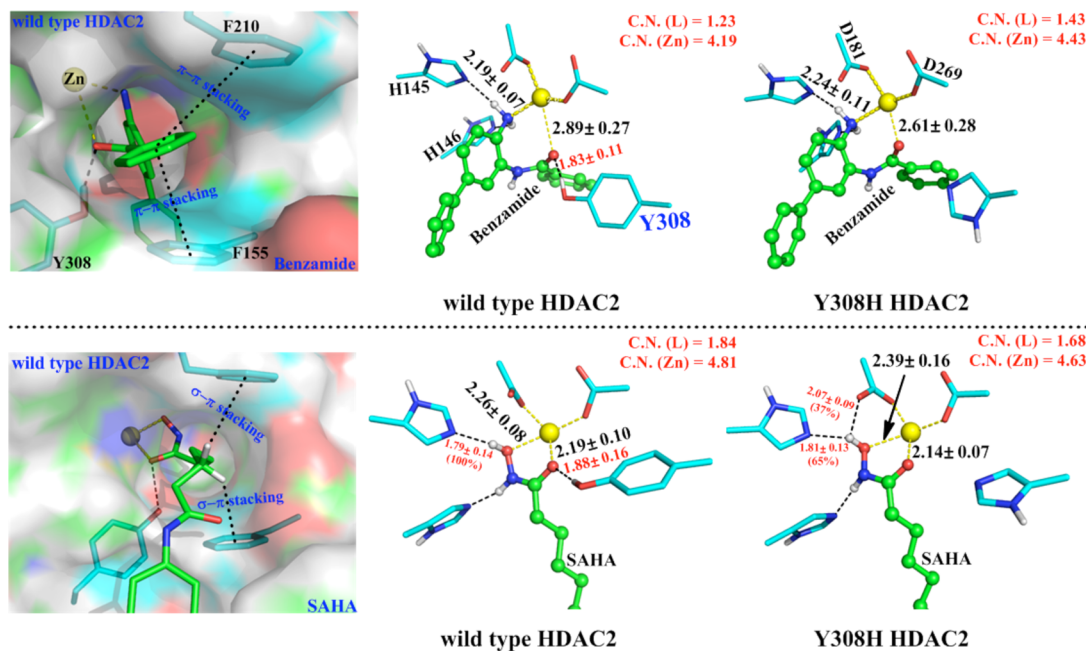


Figure 3. Different π -stacking conformations and the Y308 mutation effect in HDAC-hydroxamate and HDAC-benzamide complexes. C.N.(Zn) means the total coordination number for zinc ion, while C.N.(L) refers to the total coordination number between zinc ion and inhibitor. C.N. was defined on the basis of a very recent analysis of the zinc enzyme structures database⁹⁹ and similar to our previous study.⁵⁵

function analysis and comparison for the common π -stacking among all class I HDACs. Thus, these studies would be very helpful in designing isoform-selective inhibitors for class I HDACs.

In this work, Born–Oppenheimer *ab initio* QM/MM MD simulations were performed on 15 class I HDACs models. The distinct π -stacking conformations have been identified among class I HDACs, by comparison of the HDAC1/2/3 selective-inhibitor benzamide and the pan-inhibitor SAHA. The correlation between the π -stacking and the tyrosine is revealed first. Furthermore, the catalytic roles of the conserved tyrosine in the deacetylation of substrate and proton transfer of SAHA in HDAC have also been demonstrated.

2. COMPUTATIONAL METHODS

2.1. Preparation of Simulation Systems. As shown in Table S1, 15 simulation models were built based on the crystal structures of each class I HDACs (HDAC1, 4BKX;⁴⁶ HDAC2, 3MAX⁴⁴ and 4LXZ;⁴⁵ HDAC3, 4A69;⁴⁸ HDAC8, 2V5W⁴⁷). The detailed preparation protocol was similar to our previous study.^{53,55,58} The TIP3P model⁵⁹ and Amber99SB force field^{60–62} were employed for water molecules and the proteins, respectively, while the force field parameters of ligands (benzamide, chalcone, SAHA, and acetyl lysine) were generated from AMBER GAFF force field.⁶³ The partial atomic charges of these ligands were obtained from the restrained electrostatic potential (RESP) charge at the HF/6-31G* level with the Gaussian09 package.⁶⁴

The heating MD simulation was performed from 0 to 300 K gradually under the NVT ensemble for 50 ps. Then 100 ps MD simulations were performed under the NPT ensemble to relax the system density to be about 1.0 g/cm³, with the target temperature of 300 K and the target pressure of 1.0 atm, and then further equilibrated for ~50 ns by employing GPU-accelerated AMBER 12.0 package.⁶⁵ The MD trajectories were stable after ~5 ns, and the resulting final snapshots were

employed for subsequent QM/MM calculations.^{66–72} During the MD simulations, the SHAKE algorithm⁷³ was applied to constrain all hydrogen-containing bonds with a tolerance of 10⁻⁵. The Berendsen thermostat⁷⁴ method was used to control the system temperature, and a cutoff of 12 Å was set for both van der Waals and electrostatic interactions.

2.2. Born–Oppenheimer *ab Initio* QM/MM MD Simulations. Each cubic system from molecular dynamics (MD) simulations was cut into a sphere by removing the solvent water molecules which were beyond 30 Å of the zinc ion in the active site. The resulting systems were then partitioned into QM and MM subsystems. The structures of HDAC1/2/3/8 are highly similar, especially when they share the same residues and crystal water around the zinc coordinate shell. Therefore, the HDAC2 model was chosen as an example to illustrate the QM partition. Asp181, His183, Asp269, ligands, and zinc ion in HDAC2 models were chosen as the QM subsystem treated by B3LYP combining with the Stuttgart ECP/basis set (SDD) for the zinc atom and the 6-31G* basis set for the other QM atoms. All the left atoms were described by the Amber99SB force field, employing 18 and 12 Å cutoffs for electrostatic and van der Waals interactions, respectively. The atoms more than 20 Å away from the zinc atom were fixed. The detailed QM/MM partition was shown in Figure S1, and the QM/MM boundaries were described by the pseudobond approach^{75–78} with the improved pseudobond parameters. There was no cutoff for electrostatic interactions between QM and MM regions. The prepared QM/MM systems were first minimized, and then 25 ps QM/MM MD simulations were performed with the time step of 1 fs and the Beeman algorithm⁷⁹ to integrate the Newton equations of motion as well as the Berendsen thermostat method⁷⁴ to control the system temperature at 300 K. The configurations of the last 20 ps were collected for data analysis. All *ab initio* QM/MM calculations were performed with modified QChem-Tinker programs.^{80,81}

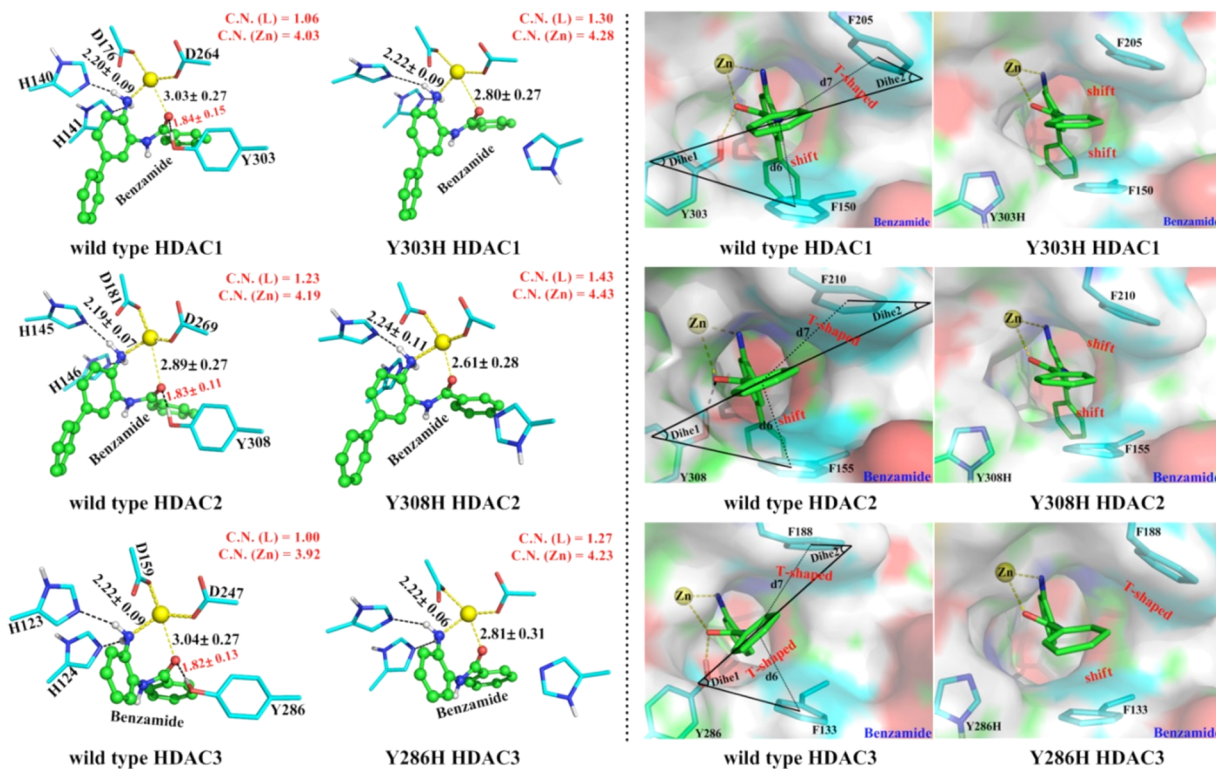


Figure 4. Illustration of the zinc-chelation modes, hydrogen-bond network in the binding pocket, and representative π - π stacking conformation near the entrance of the binding pocket for each HDAC1/2/3-benzamide model from our QM/MM MD simulations. The d6, d7, Dihe1, and Dihe2 mean the centroid distances/dihedrals between benzene rings, respectively, and they were chosen to determine the type of π - π stacking. The detailed distributions of d6, d7, Dihe1, and Dihe2 in each model were summarized in Figures S4–S5 and Table S2.

2.3. Determination of the Reaction Free Energy Profiles.

To study the hydrogen transfer from SAHA to His145 in the HDAC2-SAHA model as well as the deacetylation reaction in the HDAC8-acetyl-lysine model each prepared QM/MM system was first minimized by QM/MM optimization, and then \sim 10 ps QM/MM MD simulations were employed. The resulting structures were finally minimized to map out the minimum energy paths with the reaction coordinate driving method.⁷⁷ The determination of the reaction coordinate was consistent with our previous choice.^{53,55} For each determined structure along the reaction path, the MM subsystem was further equilibrated with 500 ps classical MD simulation with the QM subsystem fixed. Then each resulting snapshot was employed as the starting structure to carry out 25 ps *ab initio* QM/MM MD simulations with umbrella sampling.^{82,83} The configurations of the last 20 ps for each window were collected for data analysis. The probability distributions along the reaction coordinate were determined for each window and pieced together with WHAM^{84,85} to map out the free energy profile along the reaction coordinate. This computational protocol has successfully been applied to study several enzymes as well as chemical reactions in aqueous solution.^{58,86–93}

3. RESULTS AND DISCUSSION

3.1. The Different π -Stacking and Hydrogen-Bond Effect in HDAC2 for the Pan-Inhibitor SAHA and Selective-Inhibitor Benzamide. SAHA is a well-known pan-inhibitor against all class I HDACs (HDAC1/2/3/8), whereas benzamide shows a selective inhibitory effect on HDAC1/2/3 even HDAC1/2.^{2,57} In our previous study,⁵⁵

structure–function analyses of the two conserved phenylalanines in HDAC8-SAHA models have been discussed. Herein, the QM/MM MD simulations on the two other models, including wild-type and F155A/F210A double mutant HDAC2-benzamide complexes, were performed to further explore the structure–function of the two conserved phenylalanines. As shown in Figure S2, it is confirmed that two conserved phenylalanines could serve as a gating factor to prevent water molecules entering into the binding pocket in the wild-type model, leading to the higher coordinative ability for zinc in comparison to the double mutant, which has also been found in our previous QM/MM MD simulations on the HDAC8-SAHA complex.⁵⁵ Once the π -stacking is destroyed, more water molecules would enter the linker binding channel (as shown in Figure S2 and Figure S6) to decrease the positive charge of Zn^{2+} . As a result, Zn^{2+} coordinative ability was decreased.

Further comparison studies have been carried out; as depicted in Figure 3, the two stable π - π stackings between benzamide and F155 as well as F210 are well maintained in the benzamide-binding HDAC2 in our QM/MM MD simulations, while it is instead by stable σ - π stacking in the SAHA-binding HDAC2 due to the absence of the aromatic ring in the linker of SAHA. Moreover, the coordinative ability of the Zn^{2+} is increased in the HDAC2-benzamide complex by the Y308H mutant, with the average coordination distances between benzamide:O and zinc ion being significantly decreased by about 0.3 Å compared to the wild-type models; both total coordination numbers (C.N.) of zinc and the C.N. with benzamide are increased by about 0.2, thus the binding ability of benzamide is transferred to be stronger via the Y308H

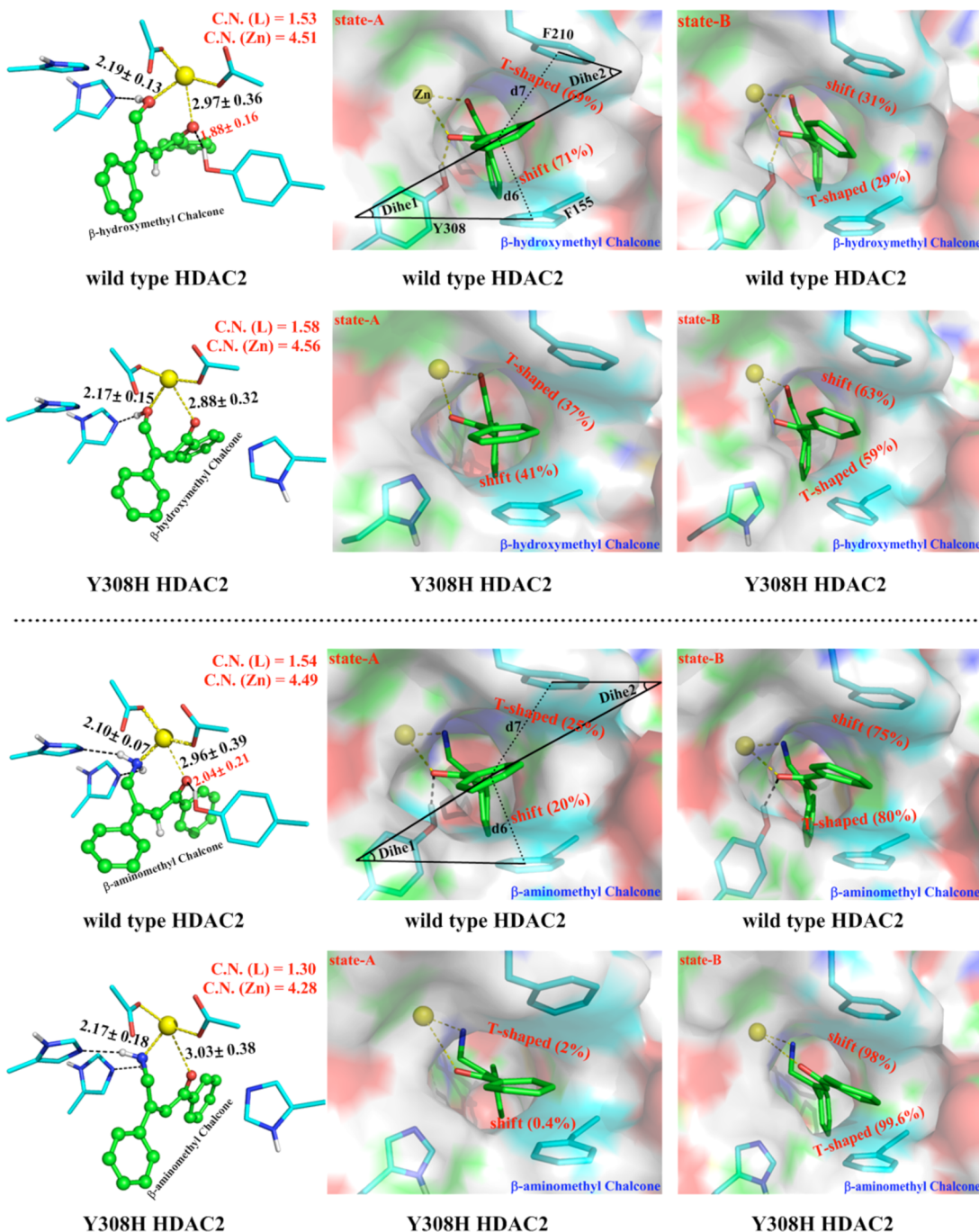


Figure 5. Illustration of the zinc-ligand chelation modes, hydrogen-bond network in the binding pocket, and representative $\pi-\pi$ stacking conformations near the entrance of the binding pocket for each HDAC2-chalcone model from our QM/MM MD simulations. The detailed distributions of d6, d7, Dihel1, and Dihel2 in each model were summarized in Figure S7 and Table S3.

mutant (see Figure 3). In contrast, the total C.N. of zinc ion and the C.N. with SAHA decreases by about 0.2 in the HDAC2-SAHA complex by the Y308H mutant (see Figure 3). Moreover, the hydrogen bond between H145 and the hydroxyl of SAHA becomes flexible, while it is very stable in the HDAC2-benzamide complex, as shown in Figure 3.

To explain the unexpected opposite phenomenon that the zinc coordinative ability increases for benzamide whereas it decreases for SAHA in Y308H HDAC2, we proposed that the distinct π stacking ($\pi-\pi$ stacking for benzamide and $\sigma-\pi$ stacking for SAHA) is associated with the absence or presence of the hydrogen bond between the ligand (SAHA or

benzamide) and conserved Y308. Considering benzamide present selective inhibition on HDAC1/2/3 but not HDAC8, further QM/MM simulations are performed to reveal the Y308H mutant effect on $\pi-\pi$ stacking among benzamide binding HDAC1/2/3 (*vide infra*).

3.2. Diversity of the $\pi-\pi$ Stacking Is Correlated with the Conserved Tyrosine for Benzamide-like Inhibitors in HDAC1/2/3. As summarized in Figures 4 and S3, benzamide prefers to form parallel shift $\pi-\pi$ stacking with F150 in the HDAC1-benzamide complex either in wild-type or the Y303H mutant model, while the T-shaped $\pi-\pi$ stacking with F205 is transferred to the parallel shift $\pi-\pi$ stacking via the Y303H

mutant. Moreover, the same phenomenon is observed in the HDAC2-benzamide complex, and the similar $\pi-\pi$ stacking conformation change for F133 is revealed in the HDAC3-benzamide complex. In comparison to the T-shaped $\pi-\pi$ stacking, the hydrophobicity of the active pocket is increased with the parallel shift $\pi-\pi$ stacking conformation, owing to the water number near the binding channel being reduced and the positive charges on zinc ion being enhanced, as shown in Figures S6 and 8(a). Due to the higher positive charge on zinc ion, the absence of the hydrogen bond by the mutating tyrosine to histidine would strengthen the zinc-benzamide chelation interaction, as highlighted in red in Figure 4, and the mutation leads to a much higher C.N. both for zinc ion and ligands in HDAC1/2/3.

The next essential issue is what is the inner molecular basis for the π -stacking regulated by the conserved tyrosine Y308. As shown in Figure 4, the $\pi-\pi$ stacking is more preferred to be the T-shape conformation in wild-type models, while the shift conformation is more popular in Y308H mutant models. Herein, we proposed that benzamide is restricted by the strong hydrogen bond interaction (the hydrogen bond length is about 1.8 Å, see Figure 4), due to the presence of the conserved tyrosine, leading to the unfavorable T-shaped $\pi-\pi$ stacking. While the restraint is missed by the Tyr mutation, it is probably favorable for formation of the shift $\pi-\pi$ stacking. This hypothesis on the correlation between the conserved tyrosine and $\pi-\pi$ stacking could be further found in HDAC2-chalcone complexes, in which the chelator and linker are very similar to benzamide.⁹⁴ As shown in Figure 5, two kinds of $\pi-\pi$ stacking states are observed either in wild-type or mutant HDAC2-chalcone models, which is not observed in the HDAC2-benzamide complex. For the β -hydroxymethyl chalcone, it prefers to form parallel shift $\pi-\pi$ stacking with F155 and T-shaped $\pi-\pi$ stacking with F210 in wild-type models, namely “state A”, but the T-shaped $\pi-\pi$ stacking with F155 and parallel shift $\pi-\pi$ stacking with F210 (namely “state B”) is more prevalent in the mutant type. Since the ratio of states A and B is about 7:3 in wild-type models while 4:6 in mutant-type models, the reverse transferability between the two $\pi-\pi$ stacking states is increased via the Y308H mutant. Due to the transferable $\pi-\pi$ stacking effect, the entrance of water from the linker binding channel would be well prevented, leading to the higher positive charge on zinc ion, as shown in Figures S8 and 8(b). Thus, the coordinative ability is increased slightly in Y308H HDAC2 (see Figure 5). In contrast, for β -aminomethyl chalcone, because of the ratio of states A and B is 2:8, the transformation of the two $\pi-\pi$ stacking states is still possible in wild-type models, but the transformation is almost impossible by the Y308H mutation (only state B exists, see Figure 5). As a result, the water number near the binding pocket increases and less positive charge on the zinc ion is observed (see Figure S8), leading to the lower zinc coordinative ability in Y308H HDAC (see Figure 5).

Therefore, the diverse $\pi-\pi$ stacking styles as well as their intertransformations in benzamide-binding HDAC1/2/3 are correlated with the conserved tyrosine, which is revealed first via our QM/MM MD simulations. The flexible $\pi-\pi$ stacking would affect the hydrophilicity of the active pocket to modulate the coordinative ability of zinc ion. Thus, the following interesting issue is what are the regulatory roles for the conserved tyrosine in the SAHA-binding HDACs (*vide infra*).

3.3. The Catalytic Role of the Conserved Tyrosine for Substrate and SAHA. As shown in Figure 6, the free energy barrier increased about 7 kcal/mol for the rate-limiting step in

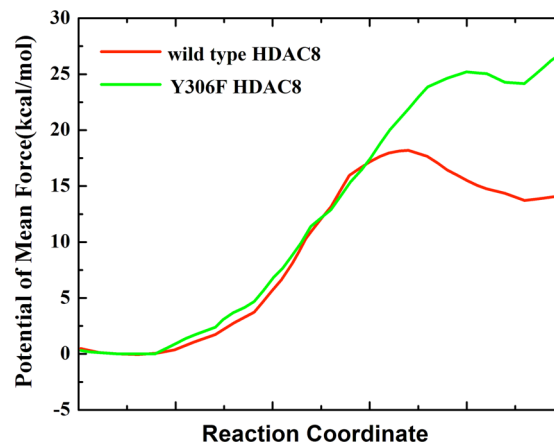


Figure 6. Free energy profiles for the rate-limiting step of deacetylation reaction in HDAC8.

the deacetylation reaction catalyzed by Y306F HDAC8 in comparison to the wild-type HDAC8, and the intermediate is unstable since it shows an endothermicity of about 25 kcal/mol. Therefore, it indicates that the conserved Y306 plays an important catalytic role in stabilizing the oxyanion at the transition state and the intermediate state. The unfavorable kinetic and thermodynamic characteristics coming from the Y306F mutation would inactivate the enzymatic catalysis, which is in agreement with the experiments that the Y306F mutation in HDAC8 decreases the catalytic activity about 4-fold,⁴⁷ while the reaction barrier is about 18 kcal/mol and the intermediate is metastable in wild-type HDAC8 (see Figure 6).⁵³ Therefore, the conserved Y306 plays an important catalytic role in stabilizing the oxyanion at the transition state and intermediate state. As shown in Figure 2, due to the existence of Y306, the highly negative charges on the oxyanion at the transition state and intermediate state would be well diffused via the hydrogen bond.

The similar catalytic role is observed in the controversial proton transfer reaction of SAHA, as shown in Figures 7 and S9, and the conserved tyrosine could also stabilize the transition state and product state. The proton transfer reaction is thermodynamically unfavorable even though it is kinetically facile in wild-type models, thus SAHA prefers to be protonated

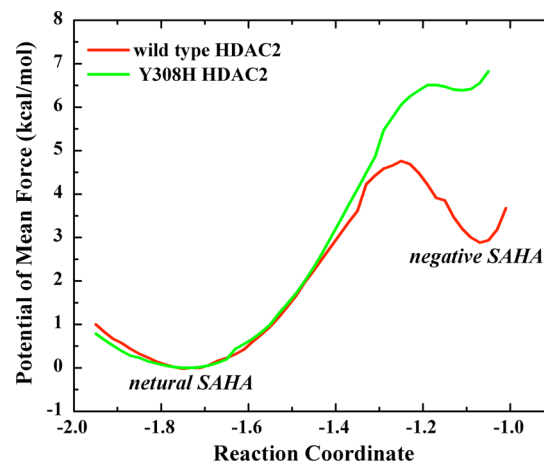


Figure 7. Free energy profiles for the proton transfer from SAHA to His145 in HDAC2. The distance between H145:N^e and SAHA:H1 was chosen as the reaction coordinate.

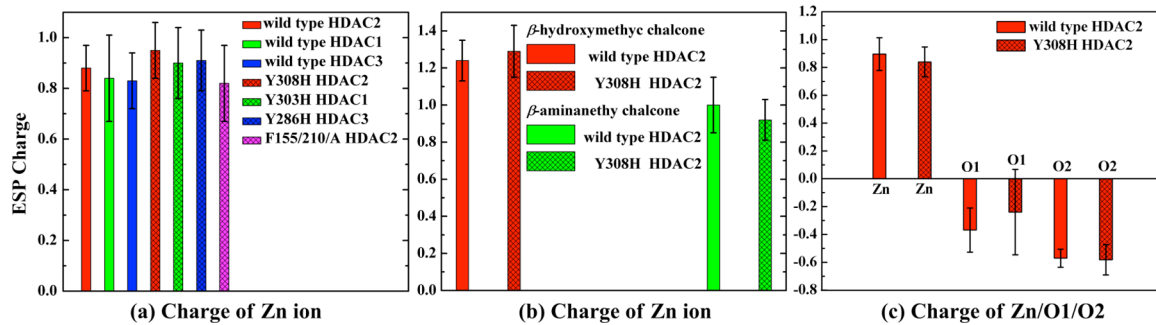


Figure 8. Average ESP charges for the selected atoms in wild-type and Tyr mutant models.

(named neutral SAHA) in wild-type HDAC2, which is consistent with the results from our previous QM/MM MD simulations⁵⁵ (25 ps QM/MM MD simulation for each window along the reaction coordinate) but inconsistent with the results from Wiest's ONIOM calculation⁹⁵ in wild-type HDAC8, in which only static QM/MM optimization with a larger QM region was performed but without MD simulations. Moreover, it should be noted that the key metal ion (K^+) located about 7 Å from the catalytic Zn^{2+} ion was neglected in Wiest's modeling, while it is thought to have an important effect on the catalytic activity.^{70,96–98} Therefore, we proposed that further more extensive QM/MM MD simulations with various combinations of QM region in different isoforms are required to finally clarify the protonation state of SAHA among all HDACs, and it is beyond the current scope of this work which focuses on the catalytic role of Tyr. As shown in Figure 3, Y308 would increase the hydrogen bond interaction between SAHA and H145, which promotes the proton transfer from SAHA to the conserved H145 and then increases the chelating ability of SAHA. The hydrogen bond becomes flexible (with D181 and H145 at percentage of 37% and 63%, respectively) and weaker (with H145) via the Y308H mutation. As a result, the proton transfer would be totally unachievable (Figure 7). Meanwhile, the chelating ability of SAHA is decreased due to the less negative charge on the coordinating atoms O1 (with big fluctuation) in the chelator of SAHA (see Figure 8(c)) as well as tiny less positive charge on zinc ion and without distinctness for the O2 atom in SAHA.

In sum, the reverse effect on the chelation of zinc-inhibitor (benzamide and SAHA) from the Y308H mutation (see Figure 3) is ascribed to their different regulation mechanisms. For benzamide-like inhibitors, the presence or absence of Y308 is correlated with the diversity of the $\pi-\pi$ stacking, which could indirectly modulate the water gating effect as well as the positive charge on the zinc ion, and then affect the coordinative ability of zinc ion. For SAHA-like inhibitors, Y308 could strengthen the hydrogen bond interaction between SAHA and H145, which would directly increase the negative charge on hydroxyl oxygen of SAHA, and then strengthen the chelating ability of SAHA.

4. CONCLUSIONS

On the basis of extensive Born–Oppenheimer *ab initio* QM/MM MD simulations on the wild-type and mutant class I HDACs models, the distinct functional roles of the conserved tyrosine (Y303/308/286/306 in HDAC1/2/3/8, respectively) in modulating the zinc-inhibitor chelation have been revealed. For HDAC1/2/3 selective-inhibitor benzamide, the diverse $\pi-\pi$ stacking (various combinations of parallel shift and T-

shaped), which are formed by the aromatic ring in benzamide and the two conserved phenylalanine residues (F150/205 in HDAC1, F155/210 in HDAC2, F133/188 in HDAC3) in the linker binding channel, could play gating roles to modulate the entrance of water molecules in the active pocket as well as effect the hydrophilicity of the active pocket among class I HDACs and thus further affect the coordinative ability of zinc ion. Moreover, the relationship between the diverse $\pi-\pi$ stacking and the conserved tyrosine is revealed first. For pan-inhibitor SAHA, the conserved tyrosine residue (namely Y308/306 in HDAC2/8) would promote the proton transfer reaction of SAHA by enhancing the hydrogen bond interaction between the protein–ligand as well as the negative charge on the hydroxyl oxygen and thus bringing the higher chelating ability of SAHA. Furthermore, our QM/MM MD simulations indicated that the conserved tyrosine also plays a critical role in stabilizing the transition state and intermediate during the deacetylation reaction of the substrate. These findings would be very helpful for further rational drug design to increase the isoform-selectivity of inhibitors among class I HDACs.

■ ASSOCIATED CONTENT

S Supporting Information

Computational models; the detailed geometry factors for the $\pi-\pi$ stacking conformations in the select models; QM/MM partition schemes; illustration of zinc chelation in the binding pocket of wild- and mutant type HDAC2; the relevance between the $\pi-\pi$ stacking styles and the selected distances in each HDAC1/2/3-benzamide model; detailed distributions of Dihe1, Dihe2, d6, and d7 in each model; the average number of water molecules near the binding pocket in each model. This material is available free of charge via the Internet at <http://pubs.acs.org>.

■ AUTHOR INFORMATION

Corresponding Authors

* E-mail: wurb3@mail.sysu.edu.cn.

*E-mail: luohb77@mail.sysu.edu.cn.

Notes

The authors declare no competing financial interest.

■ ACKNOWLEDGMENTS

This work was supported by the National Science Foundation of China (21203257, 21272289, 21103234, and 81373258) and the Guangdong Natural Science Foundation (S2011030003190 and S2013010014867). We thank the National Supercomputing Centers in Shenzhen and Guangzhou for providing the computational resources. We also thank Prof. Yingkai Zhang

and Dr. Shenglong Wang at NYU for their helps in using QChem-Tinker.

■ REFERENCES

- (1) Cole, P. A. Chemical Probes for Histone-Modifying Enzymes. *Nat. Chem. Biol.* **2008**, *4*, 590–597.
- (2) Cress, W. D.; Seto, E. Histone Deacetylases, Transcriptional Control, and Cancer. *J. Cell Physiol.* **2000**, *184*, 1–16.
- (3) Glazkova, M. A.; Sengupta, N.; Zhang, X.; Seto, E. Acetylation and Deacetylation of Non-Histone Proteins. *Gene* **2005**, *363*, 15–23.
- (4) Kouzarides, T. Chromatin Modifications and Their Function. *Cell* **2007**, *128*, 693–705.
- (5) Yuan, Z. L.; Guan, Y. J.; Chatterjee, D.; Chin, Y. E. Stat3 Dimerization Regulated by Reversible Acetylation of a Single Lysine Residue. *Science* **2005**, *307*, 269–273.
- (6) Erickson, P.; Gao, J.; Chang, K. S.; Look, T.; Whisenant, E.; Raimondi, S.; Lasher, R.; Trujillo, J.; Rowley, J.; Drabkin, H. Identification of Breakpoints in t(8;21) Acute Myelogenous Leukemia and Isolation of a Fusion Transcript, AML1/ETO, with similarity to Drosophila Segmentation Gene, runt. *Blood* **1992**, *80*, 1825–1831.
- (7) Hug, B. A.; Lazar, M. A. ETO Interacting Proteins. *Oncogene* **2004**, *23*, 4270–4274.
- (8) Arrowsmith, C. H.; Bountra, C.; Fish, P. V.; Lee, K.; Schapira, M. Epigenetic Protein Families: a new Frontier for Drug Discovery. *Nat. Rev. Drug Discovery* **2012**, *11*, 384–400.
- (9) Baylin, S. B.; Jones, P. A. A decade of exploring the Cancer Epigenome - Biological and Translational Implications. *Nat. Rev. Cancer* **2011**, *11*, 726–734.
- (10) Gräff, J.; Kim, D.; Dobbin, M. M.; Tsai, L. H. Epigenetic Regulation of Gene Expression in Physiological and Pathological brain processes. *Physiol. Rev.* **2011**, *91*, 603–649.
- (11) McKinsey, T. A. Isoform-Selective HDAC Inhibitors: Closing in on Translational Medicine for the heart. *J. Mol. Cell. Cardiol.* **2011**, *51*, 491–496.
- (12) Shakespear, M. R.; Halili, M. A.; Irvine, K. M.; Fairlie, D. P.; Sweet, M. J. Histone Deacetylases as Regulators of Inflammation and Immunity. *Trends Immunol.* **2011**, *32*, 335–343.
- (13) Wiech, N. L.; Fisher, J. F.; Helquist, P.; Wiest, O. Inhibition of Histone Deacetylases: A Pharmacological Approach to the Treatment of Non-Cancer Disorders. *Curr. Top. Med. Chem.* **2009**, *9*, 257–271.
- (14) Chuang, D. M.; Leng, Y.; Marinova, Z.; Kim, H. J.; Chiu, C. T. Multiple roles of HDAC Inhibition in Neurodegenerative Conditions. *Trends Neurosci.* **2009**, *32*, 591–601.
- (15) Guidotti, A.; Auta, J.; Chen, Y.; Davis, J. M.; Dong, E.; Gavin, D. P.; Grayson, D. R.; Matrisiano, F.; Pinna, G.; Satta, R.; Sharma, R. P.; Tremolizzo, L.; Tueting, P. Epigenetic GABAergic Targets in Schizophrenia and Bipolar Disorder. *Neuropharmacology* **2011**, *60*, 1007–1016.
- (16) Shahbazian, M. D.; Grunstein, M. Functions of Site-Specific Histone Acetylation and Deacetylation. *Annu. Rev. Biochem.* **2007**, *76*, 75–100.
- (17) Bolden, J. E.; Peart, M. J.; Johnstone, R. W. Anticancer Activities of Histone Deacetylase Inhibitors. *Nat. Rev. Drug Discovery* **2006**, *5*, 769–784.
- (18) Gottesfeld, J. M.; Rusche, J. R.; Pandolfo, M. Increasing Frataxin Gene Expression with Histone Deacetylase Inhibitors as a Therapeutic Approach for Friedreich's ataxia. *J. Neurochem.* **2013**, *126*, 147–154.
- (19) Haberland, M.; Montgomery, R. L.; Olson, E. N. The many roles of Histone Deacetylases in Development and Physiology: Implications for Disease and Therapy. *Nat. Rev. Genet.* **2009**, *10*, 32–42.
- (20) Helquist, P.; Maxfield, F. R.; Wiech, N. L.; Wiest, O. Treatment of Niemann-Pick Type C Disease by Histone Deacetylase Inhibitors. *Neurotherapeutics* **2013**, *10*, 688–697.
- (21) Kazantsev, A. G.; Thompson, L. M. Therapeutic Application of Histone Deacetylase Inhibitors for Central Nervous System Disorders. *Nat. Rev. Drug Discovery* **2008**, *7*, 854–868.
- (22) Minucci, S.; Pellicci, P. G. Histone Deacetylase Inhibitors and the Promise of Epigenetic (and more) Treatments for Cancer. *Nat. Rev. Cancer* **2006**, *6*, 38–51.
- (23) Paris, M.; Porcelloni, M.; Binasci, M.; Fattori, D. Histone Deacetylase Inhibitors: From Bench to Clinic. *J. Med. Chem.* **2008**, *51*, 1505–1529.
- (24) Soragni, E.; Xu, C.; Plasterer, H. L.; Jacques, V.; Rusche, J. R.; Gottesfeld, J. M. Rationale for the Development of 2-aminobenzamide Histone Deacetylase Inhibitors as Therapeutics for Friedreich ataxia. *J. Child. Neurol.* **2012**, *27*, 1164–1173.
- (25) Jones, A. P.; Haynes, R.; Harvey, I. M.; Jewell, T. Road Traffic Crashes and the Protective Effect of Road Curvature over small areas. *Health Place* **2012**, *18*, 315–320.
- (26) Lane, A. A.; Chabner, B. A. Histone Deacetylase Inhibitors in Cancer Therapy. *J. Clin. Oncol.* **2009**, *27*, 5459–5468.
- (27) Ma, X.; Ezzeldin, H. H.; Diasio, R. B. Histone Deacetylase Inhibitors Current Status and Overview of Recent Clinical Trials. *Drugs* **2009**, *69*, 1911–1934.
- (28) Wang, C.; Flemming, C. J.; Cheng, Y. Q. Discovery and Activity Profiling of Thailandeepsins A through F, Potent Histone Deacetylase Inhibitors, from Burkholderia Thailandensis E264. *MedChemComm* **2012**, *3*, 976–981.
- (29) Wang, C.; Henkes, L. M.; Doughty, L. B.; He, M.; Wang, D.; Meyer-Almes, F. J.; Cheng, Y. Q. Thailandeepsins: Bacterial Products with Potent Histone Deacetylase Inhibitory Activities and Broad-Spectrum Antiproliferative Activities. *J. Nat. Prod.* **2011**, *74*, 2031–2038.
- (30) Duvic, M.; Talpur, R.; Ni, X.; Zhang, C.; Hazarika, P.; Kelly, C.; Chiao, J. H.; Reilly, J. F.; Ricker, J. L.; Richon, V. M.; Frankel, S. R. Phase 2 trial of Oral Vorinostat (Suberoylanilide Hydroxamic Acid, SAHA) for Refractory Cutaneous T-cell Lymphoma (CTCL). *Blood* **2007**, *109*, 31–39.
- (31) FDA. StatBite: FDA Oncology Drug Product Approvals in 2009. *J. Natl. Cancer Inst.* **2010**, *102*, 219.
- (32) Mann, B. S.; Johnson, J. R.; Cohen, M. H.; Justice, R.; Pazdur, R. FDA Approval Summary: Vorinostat for Treatment of Advanced Primary Cutaneous T-cell Lymphoma. *Oncologist* **2007**, *12*, 1247–1252.
- (33) Bradner, J. E.; West, N.; Grachan, M. L.; Greenberg, E. F.; Haggarty, S. J.; Warnow, T.; Mazitschek, R. Chemical Phylogenetics of Histone Deacetylases. *Nat. Chem. Biol.* **2010**, *6*, 238–243.
- (34) Dokmanovic, M.; Clarke, C.; Marks, P. A. Histone Deacetylase Inhibitors: Overview and Perspectives. *Mol. Cancer Res.* **2007**, *5*, 981–989.
- (35) Frumm, S. M.; Fan, Z. P.; Ross, K. N.; Duvall, J. R.; Gupta, S.; VerPlank, L.; Suh, B. C.; Holson, E.; Wagner, F. F.; Smith, W. B.; Paranal, R. M.; Bassil, C. F.; Qi, J.; Roti, G.; Kung, A. L.; Bradner, J. E.; Tolliday, N.; Stegmaier, K. Selective HDAC1/HDAC2 Inhibitors induce Neuroblastoma Differentiation. *Chem. Biol.* **2013**, *20*, 713–725.
- (36) Hamblett, C. L.; Methot, J. L.; Mampreian, D. M.; Sloman, D. L.; Stanton, M. G.; Kral, A. M.; Fleming, J. C.; Cruz, J. C.; Chenard, M.; Ozerova, N.; Hitz, A. M.; Wang, H.; Deshmukh, S. V.; Nazeef, N.; Harsch, A.; Hughes, B.; Dahlberg, W. K.; Szewczak, A. A.; Middleton, R. E.; Mosley, R. T.; Sechrist, J. P.; Miller, T. A. The Discovery of 6-amino Nicotinamides as Potent and Selective Histone Deacetylase Inhibitors. *Bioorg. Med. Chem. Lett.* **2007**, *17*, 5300–5309.
- (37) Karagiannis, T. C.; El-Osta, A. Will Broad-Spectrum Histone Deacetylase Inhibitors be superseded by more Specific Compounds? *Leukemia* **2007**, *21*, 61–65.
- (38) Miller, T. A.; Witter, D. J.; Belvedere, S. Histone Deacetylase Inhibitors. *J. Med. Chem.* **2003**, *46*, S097–S116.
- (39) Zhang, Y.; Fang, H.; Feng, J.; Jia, Y.; Wang, X.; Xu, W. Discovery of a Tetrahydroisoquinoline-based Hydroxamic Acid Derivative (ZYJ-34c) as Histone Deacetylase Inhibitor with Potent Oral Antitumor Activities. *J. Med. Chem.* **2011**, *54*, 5532–5539.
- (40) Allis, C. D.; Berger, S. L.; Cote, J.; Dent, S.; Jenuwien, T.; Kouzarides, T.; Pillus, L.; Reinberg, D.; Shi, Y.; Shiekhattar, R.; Shilatifard, A.; Workman, J.; Zhang, Y. New Nomenclature for Chromatin-Modifying Enzymes. *Cell* **2007**, *131*, 633–636.

- (41) Subramanian, S.; Bates, S. E.; Wright, J. J.; Espinoza-Delgado, I.; Piekarz, R. L. Clinical Toxicities of Histone Deacetylase Inhibitors. *Pharmaceuticals* **2010**, *3*, 2751–2767.
- (42) Hildmann, C.; Riester, D.; Schwienhorst, A. Histone Deacetylases—an important Class of Cellular Regulators with a Variety of Functions. *Appl. Microbiol. Biotechnol.* **2007**, *75*, 487–497.
- (43) Marks, P. A.; Breslow, R. Dimethyl Sulfoxide to Vorinostat: Development of this Histone Deacetylase Inhibitor as an Anticancer Drug. *Nat. Biotechnol.* **2007**, *25*, 84–90.
- (44) Bressi, J. C.; Jennings, A. J.; Skene, R.; Wu, Y.; Melkus, R.; De Jong, R.; O'Connell, S.; Grimshaw, C.; Navre, M.; Gangloff, A. R. Exploration of the HDAC2 Foot Pocket: Synthesis and SAR of substituted N-(2-aminophenyl)Benzamides. *Bioorg. Med. Chem. Lett.* **2010**, *20*, 3142–3145.
- (45) Lauffer, B. E.; Mintzer, R.; Fong, R.; Mukund, S.; Tam, C.; Zilberleyb, I.; Flicke, B.; Ritscher, A.; Fedorowicz, G.; Vallero, R.; Ortwine, D. F.; Gunzner, J.; Modrusan, Z.; Neumann, L.; Koth, C.; Lupardus, P. J.; Kaminker, J. S.; Heise, C. E.; Steiner, P. Histone Deacetylase (HDAC) Inhibitor Kinetic Rate Constants correlate with Cellular Histone Acetylation but not Transcription and Cell Viability. *J. Biol. Chem.* **2013**, *288*, 26926–26943.
- (46) Millard, C. J.; Watson, P. J.; Celardo, I.; Gordiyenko, Y.; Cowley, S. M.; Robinson, C. V.; Fairall, L.; Schwabe, J. W. Class I HDACs share a Common Mechanism of Regulation by Inositol Phosphates. *Mol. Cell* **2013**, *51*, 57–67.
- (47) Vannini, A.; Volpari, C.; Gallinari, P.; Jones, P.; Mattu, M.; Carfi, A.; De Francesco, R.; Steinkühler, C.; Di Marco, S. Substrate Binding to Histone Deacetylases as shown by the Crystal Structure of the HDAC8-Substrate Complex. *EMBO Rep.* **2007**, *8*, 879–884.
- (48) Watson, P. J.; Fairall, L.; Santos, G. M.; Schwabe, J. W. Structure of HDAC3 Bound to Co-Repressor and Inositol Tetraphosphate. *Nature* **2012**, *481*, 335–340.
- (49) Wambua, M. K.; Nalawansha, D. A.; Negmeldin, A. T.; Pflum, M. K. Mutagenesis Studies of the 14 Å Internal Cavity of Histone Deacetylase 1: Insights toward the Acetate-Escape Hypothesis and Selective Inhibitor Design. *J. Med. Chem.* **2014**, *57*, 642–650.
- (50) Bottomley, M. J.; Lo Surdo, P.; Di Giovine, P.; Cirillo, A.; Scarpelli, R.; Ferrigno, F.; Jones, P.; Neddermann, P.; De Francesco, R.; Steinkuhler, C.; Gallinari, P.; Carfi, A.; Bottomley, M. J.; Lo Surdo, P.; Di Giovine, P.; Cirillo, A.; Scarpelli, R.; Ferrigno, F.; Jones, P.; Neddermann, P.; De Francesco, R.; Steinkuhler, C.; Gallinari, P.; Carfi, A. Structural and Functional Analysis of the Human HDAC4 Catalytic Domain reveals a Regulatory Structural Zinc-Binding Domain. *J. Biol. Chem.* **2008**, *283*, 26694–26704.
- (51) Lahm, A.; Paolini, C.; Pallaoro, M.; Nardi, M. C.; Jones, P.; Neddermann, P.; Sambucini, S.; Bottomley, M. J.; Lo Surdo, P.; Carfi, A.; Koch, U.; De Francesco, R.; Steinkuhler, C.; Gallinari, P. Unraveling the Hidden Catalytic Activity of Vertebrate Class IIa Histone Deacetylases. *Proc. Natl. Acad. Sci. U. S. A.* **2007**, *104*, 17335–17340.
- (52) Schuetz, A.; Min, J.; Allali-Hassani, A.; Schapira, M.; Shuen, M.; Loppnau, P.; Mazitschek, R.; Kwiatkowski, N. P.; Lewis, T. A.; Maglathin, R. L.; McLean, T. H.; Bochkarev, A.; Plotnikov, A. N.; Vedadi, M.; Arrowsmith, C. H. Human HDAC7 Harbors a Class IIa Histone Deacetylase-Specific Zinc Binding Motif and Cryptic Deacetylase Activity. *J. Biol. Chem.* **2008**, *283*, 11355–11363.
- (53) Wu, R.; Wang, S.; Zhou, N.; Cao, Z.; Zhang, Y. A Proton-Shuttle Reaction Mechanism for Histone Deacetylase 8 and the Catalytic Role of Metal Ions. *J. Am. Chem. Soc.* **2010**, *132*, 9471–9479.
- (54) Wang, D. F.; Helquist, P.; Wiest, O. Zinc Binding in HDAC Inhibitors: a DFT study. *J. Org. Chem.* **2007**, *72*, 5446–5449.
- (55) Wu, R.; Lu, Z.; Cao, Z.; Zhang, Y. Zinc Chelation with Hydroxamate in Histone Deacetylases Modulated by Water Access to the Linker Binding Channel. *J. Am. Chem. Soc.* **2011**, *133*, 6110–6113.
- (56) Weerasinghe, S. V. W.; Estiu, G.; Wiest, O.; Pflum, M. K. H. Residues in the 11 Å Channel of Histone Deacetylase 1 Promote Catalytic Activity: Implications for Designing Isoform-Selective Histone Deacetylase Inhibitors. *J. Med. Chem.* **2008**, *51*, 5542–5551.
- (57) Bertrand, P. Inside HDAC with HDAC inhibitors. *Eur. J. Med. Chem.* **2010**, *45*, 2095–2116.
- (58) Wu, R.; Hu, P.; Wang, S.; Cao, Z.; Zhang, Y. Flexibility of Catalytic Zinc Coordination in Thermolysin and HDAC8: A Born-Oppenheimer ab initio QM/MM Molecular Dynamics Study. *J. Chem. Theory Comput.* **2010**, *6*, 337–343.
- (59) Jorgensen, W. L.; Chandrasekhar, J.; Madura, J. D.; Impey, R. W.; Klein, M. L. Comparison of Simple Potential Functions for Simulating Liquid Water. *J. Chem. Phys.* **1983**, *79*, 926–935.
- (60) Cornell, W. D.; Cieplak, P.; Bayly, C. I.; Gould, I. R.; Merz, K. M.; Ferguson, D. M.; Spellmeyer, D. C.; Fox, T.; Caldwell, J. W.; Kollman, P. A. A Second Generation Force Field for the Simulation of Proteins, Nucleic Acids, and Organic Molecules. *J. Am. Chem. Soc.* **1995**, *117*, 5179–5197.
- (61) Wang, J. M.; Cieplak, P.; Kollman, P. A. Geometrical and Electronic Structure Variability of the Sugar-Phosphate Backbone in Nucleic acids. *J. Comput. Chem.* **2000**, *21*, 1049–1074.
- (62) Hornak, V.; Abel, R.; Okur, A.; Strockbine, B.; Roitberg, A.; Simmerling, C. Comparison of Multiple Amber Force Fields and Development of Improved Protein Backbone Parameters. *Proteins: Struct., Funct., Bioinf.* **2006**, *65*, 712–725.
- (63) Wang, J. M.; Wolf, R. M.; Caldwell, J. W.; Kollman, P. A.; Case, D. A. Development and Testing of a General Amber Force Field. *J. Comput. Chem.* **2004**, *25*, 1157–1174.
- (64) Frisch, M. J.; Trucks, G. W.; Schlegel, H. B.; Scuseria, G. E.; Robb, M. A.; Cheeseman, J. R.; Scalmani, G.; Barone, V.; Mennucci, B.; Petersson, G. A.; Nakatsuji, H.; Caricato, M.; Li, X.; Hratchian, H. P.; Izmaylov, A. F.; Bloino, J.; Zheng, G.; Sonnenberg, J. L.; Hada, M.; Ehara, M.; Toyota, K.; Fukuda, R.; Hasegawa, J.; Ishida, M.; Nakajima, T.; Honda, Y.; Kitao, O.; Nakai, H.; Vreven, T.; Montgomery, J. A., Jr.; Peralta, J. E.; Ogliaro, F.; Bearpark, M.; Heyd, J. J.; Brothers, E.; Kudin, K. N.; Staroverov, V. N.; Kobayashi, R.; Normand, J.; Raghavachari, K.; Rendell, A.; Burant, J. C.; Iyengar, S. S.; Tomasi, J.; Cossi, M.; Rega, N.; Millam, J. M.; Klene, M.; Knox, J. E.; Cross, J. B.; Bakken, V.; Adamo, C.; Jaramillo, J.; Gomperts, R.; Stratmann, R. E.; Yazeyev, O.; Austin, A. J.; Cammi, R.; Pomelli, C.; Ochterski, J. W.; Martin, R. L.; Morokuma, K.; Zakrzewski, V. G.; Voth, G. A.; Salvador, P.; Dannenberg, J. J.; Dapprich, S.; Daniels, A. D.; Farkas, Ö.; Foresman, J. B.; Ortiz, J. V.; Ciosowski, J.; Fox, D. J. *Gaussian09*; Gaussian, Inc.: Wallingford, CT, 2009.
- (65) Case, D. A.; Darden, T. A.; Cheatham, T. E., III; Simmerling, C. L.; Wang, J.; Duke, R. E.; Luo, R.; Walker, R. C.; Zhang, W.; Merz, K. M.; Roberts, B.; Hayik, S.; Roitberg, A.; Seabra, G.; Swails, J.; Götz, A. W.; Kolossváry, I.; Wong, K. F.; Paesani, F.; Vanicek, J.; Wolf, R. M.; Liu, J.; Wu, X.; Brozell, S. R.; Steinbrecher, T.; Gohlke, H.; Cai, Q.; Ye, X.; Wang, J.; Hsieh, M.-J.; Cui, G.; Roe, D. R.; Mathews, D. H.; Seetin, M. G.; Salomon-Ferrer, R.; Sagui, C.; Babin, V.; Luchko, T.; Gusarov, S.; Kovalenko, A.; Kollman, P. A. *AMBER 12*; University of California: San Francisco. 2012.
- (66) Warshel, A. *Computer Modelling of Chemical Reactions in Enzymes and Solutions*; John Wiley and Sons, Inc.: New York, 1991.
- (67) Olsson, M. H.; Siegbahn, P. E.; Blomberg, M. R.; Warshel, A. Exploring Pathways and Barriers for Coupled ET/PT in Cytochrome C oxidase: a General Framework for Examining Energetics and Mechanistic Alternatives. *Biochim. Biophys. Acta* **2007**, *1767*, 244–260.
- (68) Kamerlin, S. C.; Mavri, J.; Warshel, A. Examining the Case for the Effect of Barrier Compression on Tunneling, vibrationally Enhanced Catalysis, Catalytic Entropy and Related Issues. *FEBS Lett.* **2010**, *584*, 2759–2766.
- (69) Adamczyk, A. J.; Cao, J.; Kamerlin, S. C.; Warshel, A. Catalysis by Dihydrofolate Reductase and other Enzymes Arises from Electrostatic Preorganization, not Conformational Motions. *Proc. Natl. Acad. Sci. U. S. A.* **2011**, *108*, 14115–14120.
- (70) Warshel, A.; Levitt, M. Theoretical Studies of Enzymic Reactions: Dielectric, Electrostatic and Steric Stabilization of the Carbonium Ion in the reaction of Lysozyme. *J. Mol. Biol.* **1976**, *103*, 227–249.
- (71) Yue, Y.; Guo, H. Quantum Mechanical/Molecular Mechanical Study of Catalytic Mechanism and Role of Key Residues in

- Methylation Reactions Catalyzed by Dimethylxanthine Methyltransferase in Caffeine Biosynthesis. *J. Chem. Inf. Model.* **2014**, *54*, 593–600.
- (72) Elsässer, B.; Fels, G.; Weare, J. H. QM/MM Simulation (B3LYP) of the RNase A Cleavage-Transesterification Reaction Supports a Triester A(N) + D(N) Associative Mechanism with an O_{2'}H Internal Proton Transfer. *J. Am. Chem. Soc.* **2014**, *136*, 927–936.
- (73) Ryckaert, J. P.; Ciccotti, G.; Berendsen, H. J. C. Numerical Integration of the Cartesian Equations of Motion of a System with Constraints: Molecular Dynamics of N-Alkanes. *J. Comput. Phys.* **1977**, *23*, 327–341.
- (74) Berendsen, H. J. C.; Postma, J. P. M.; Van Gunsteren, W. F.; DiNola, A.; Haak, J. R. Molecular Dynamics with Coupling to an External Bath. *J. Chem. Phys.* **1984**, *81*, 3684–3690.
- (75) Zhang, Y. K. Pseudobond ab initio QM/MM Approach and its Applications to Enzyme Reactions. *Theor. Chem. Acc.* **2006**, *116*, 43–50.
- (76) Zhang, Y. K.; Lee, T. S.; Yang, W. T. A Pseudobond Approach to Combining Quantum Mechanical and Molecular Mechanical Methods. *J. Chem. Phys.* **1999**, *110*, 46–54.
- (77) Zhang, Y. K.; Liu, H. Y.; Yang, W. T. Free Energy Calculations on Enzyme Reactions with an Efficient Iterative Procedure to Determine Minimum Energy Paths on a Combined ab initio QM/MM Potential. *J. Chem. Phys.* **2000**, *112*, 3483–3492.
- (78) Zhang, Y. K. Improved Pseudobonds for Combined ab initio Quantum Mechanical/Molecular Mechanical Methods. *J. Chem. Phys.* **2005**, *122*, 024114.
- (79) Beeman, D. Some Multistep Methods for Use in Molecular Dynamics Calculations. *J. Comput. Phys.* **1976**, *20*, 130–139.
- (80) Shao, Y.; Molnar, L. F.; Jung, Y.; Kussmann, J. O. C.; Brown, S. T.; Gilbert, A. T.; Slipchenko, L. V.; Levchenko, S. V.; O'Neill, D. P.; DiStasio, R. A.; Lochan, R. C.; Wang, T.; Beran, G. J.; Besley, N. A.; Herbert, J. M.; Lin, C. Y.; Van Voorhis, T.; Chien, S. H.; Sodt, A.; Steele, R. P.; Rassolov, V. A.; Maslen, P. E.; Korambath, P. P.; Adamson, R. D.; Austin, B.; Baker, J.; Byrd, E. F.; Dachsel, H.; Doerkens, R. J.; Dreuw, A.; Dunietz, B. D.; Dutoi, A. D.; Furlani, T. R.; Gwaltney, S. R.; Heyden, A.; Hirata, S.; Hsu, C. P.; Kedziora, G.; Khaliulin, R. Z.; Klunzinger, P.; Lee, A. M.; Lee, M. S.; Liang, W.; Lotan, I.; Nair, N.; Peters, B.; Proynov, E. I.; Pieniazek, P. A.; Rhee, Y. M.; Ritchie, J.; Rosta, E.; Sherrill, C. D.; Simonett, A. C.; Subotnik, J. E.; Woodcock, H. L.; Zhang, W.; Bell, A. T.; Chakraborty, A. K.; Chipman, D. M.; Keil, F. J.; Warshel, A.; Hehre, W. J.; Schaefer, H. F.; Kong, J.; Krylov, A. I.; Gill, P. M.; Head-Gordon, M. Q-Chem, version 3.0; Q-Chem, Inc.: Pittsburgh, PA, 2006.
- (81) Ponder, J. W. TINKER, Software Tools for Molecular Design, Version 4.2; 2004.
- (82) Torrie, G. M.; Valleau, J. P. Nonphysical Sampling Distributions in Monte Carlo Free-Energy Estimation: Umbrella Sampling. *J. Comput. Phys.* **1977**, *23*, 187–199.
- (83) Vijayaraj, R.; Van Damme, S.; Bultinck, P.; Subramanian, V. Molecular Dynamics and Umbrella Sampling Study of Stabilizing Factors in Cyclic Peptide-Based Nanotubes. *J. Phys. Chem. B* **2012**, *116*, 9922–9933.
- (84) Kumar, S.; Bouzida, D.; Swendsen, R. H.; Kollman, P. A.; Rosenberg, J. M. Liquid-Liquid Transition in ST2 Water. *J. Comput. Chem.* **1992**, *13*, 1011–1021.
- (85) Souaille, M.; Roux, B. Extension to the Weighted Histogram Analysis Method: Combining Umbrella Sampling with Free Energy Calculations. *Comput. Phys. Commun.* **2001**, *135*, 40–57.
- (86) Wang, S. L.; Hu, P.; Zhang, Y. K. Ab initio Quantum Mechanical/Molecular Mechanical Molecular Dynamics Simulation of Enzyme Catalysis: the Case of Histone Lysine Methyltransferase SET7/9. *J. Phys. Chem. B* **2007**, *111*, 3758–3764.
- (87) Hu, P.; Wang, S.; Zhang, Y. How do SET-Domain Protein Lysine Methyltransferases Achieve the Methylation State Specificity? Revisited by Ab initio QM/MM Molecular Dynamics Simulations. *J. Am. Chem. Soc.* **2008**, *130*, 3806–3813.
- (88) Hu, P.; Wang, S. L.; Zhang, Y. K. Highly Dissociative and Concerted Mechanism for the Nicotinamide Cleavage Reaction in Sir2Tm Enzyme Suggested by ab initio QM/MM Molecular Dynamics Simulations. *J. Am. Chem. Soc.* **2008**, *130*, 16721–16728.
- (89) Lu, Z. Y.; Zhang, Y. K. Interfacing ab initio Quantum Mechanical Method with Classical Drude Oscillator Polarizable Model for Molecular Dynamics Simulation of Chemical Reactions. *J. Chem. Theory Comput.* **2008**, *4*, 1237–1248.
- (90) Ke, Z. H.; Wang, S. L.; Xie, D. Q.; Zhang, Y. K. Born-Oppenheimer ab initio QM/MM Molecular Dynamics Simulations of the Hydrolysis Reaction Catalyzed by Protein Arginine Deiminase 4. *J. Phys. Chem. B* **2009**, *113*, 16705–16710.
- (91) Ke, Z. H.; Zhou, Y. Z.; Hu, P.; Wang, S. L.; Xie, D. Q.; Zhang, Y. K. Active Site Cysteine is Protonated in the PAD4Michaelis Complex: Evidence from Born-Oppenheimer ab initio QM/MM Molecular Dynamics Simulations. *J. Phys. Chem. B* **2009**, *113*, 12750–12758.
- (92) Zheng, H.; Wang, S. L.; Zhang, Y. K. Increasing the Time Step with Mass Scaling in Born-Oppenheimer ab initio QM/MM Molecular Dynamics Simulations. *J. Comput. Chem.* **2009**, *30*, 2706–2711.
- (93) Chen, N.; Zhou, J.; Li, J.; Xu, J.; Wu, R. Concerted Cyclization of Lanosterol C-Ring and D-Ring Under Human Oxidosqualene Cyclase Catalysis: An ab Initio QM/MM MD Study. *J. Chem. Theory Comput.* **2014**, *10*, 1109–1120.
- (94) Wu, R. B.; Zhou, J. W.; Gu, Q. Preparation Method of a β -Substituted Chalcone Analogue and its Application in the Preparation of HDAC Inhibitors. Chinese patent, Appl. No.201310618498.3, 2013.
- (95) Chen, K.; Zhang, X.; Wu, Y. D.; Wiest, O. Inhibition and Mechanism of HDAC8 Revisited. *J. Am. Chem. Soc.* **2014**, *136*, 11636–11643.
- (96) Gantt, S. L.; Joseph, C. G.; Fierke, C. A. Activation and Inhibition of Histone Deacetylase 8 by Monovalent Cations. *J. Biol. Chem.* **2010**, *285*, 6036–6043.
- (97) Vannini, A.; Volpari, C.; Filocamo, G.; Casavola, E. C.; Brunetti, M.; Renzoni, D.; Chakravarty, P.; Paolini, C.; De Francesco, R.; Gallinari, P.; Steinkihler, C.; Di Marco, S. Crystal Structure of a Eukaryotic Zinc-Dependent Histone Deacetylase, Human HDAC8, Complexed with a Hydroxamic Acid Inhibitor. *Proc. Natl. Acad. Sci. U. S. A.* **2004**, *101*, 15064–15069.
- (98) Werbeck, N. D.; Kirkpatrick, J.; Reinstein, J.; Hansen, D. F. Using ¹⁵N-Ammonium to Characterise and Map Potassium Binding Sites in Proteins by NMR Spectroscopy. *ChemBioChem* **2014**, *15*, 543–548.
- (99) Tamames, B.; Sousa, S. F.; Tamames, J.; Fernandes, P. A.; Ramos, M. J. Analysis of Zinc-Ligand Bond Lengths in Metalloproteins: Trends and Patterns. *Proteins: Struct., Funct., Bioinf.* **2007**, *69*, 466–475.